Am J Nucl Med Mol Imaging 2019;9(2):140-155
www.ajnmmi.us /ISSN:2160-8407/ajnmmi0090321

Original Article

Quantitative applications in positron emission tomography achieved through signal modelling

Rozh H Al-Mashhadi[1,2], Lars P Tolbod[3]

Departments of [1]Clinical Medicine, [2]Radiology, [3]Nuclear Medicine and PET Center, Aarhus University Hospital, Aarhus, Denmark

Received December 23, 2018; Accepted February 28, 2019; Epub April 15, 2019; Published April 30, 2019

Abstract: Positron emission tomography (PET) is a valuable tool in medical imaging, but it provides limited quantitative utility in a number of important applications, such as mapping of tracer accumulation in small tissues and quantitative assessment of factors affecting tracer uptake. We aimed to develop a quantification approach based on signal modelling, to address the above limitations. Our signal modelling approach allows for a comprehensive description of target and background signals. We used *in silico* simulations to exemplify the quantitative utility of signal modelling in a number of applications and conducted scans of standardized PET phantoms to validate our computer simulation algorithms. The simulations showed that the modelling approach allows applications not supported by current techniques, such as estimation of activity fractions of sub-resolution small tissues and accurate quantification of the effect of biological factors, such as hypoxia, on tracer accumulation. There was strong agreement between the simulation data and actual scans of phantoms, providing support for the validity of the simulation algorithms. We conclude that the presented signal modelling approach may provide a framework for image analysis that can improve and expand the quantitative capacity of PET imaging.

Keywords: Signal model, quantitative PET, in silico, signal displacement effects, hypoxia

Introduction

Positron emission tomography (PET) is a valuable diagnostic tool that is widely used in oncology, neuroscience and cardiovascular medicine. Although the utility of PET imaging has expanded substantially in recent decades, the quantitative capacity of PET continues to be limited in a number of important applications. One principal limitation of PET is its relatively low resolution that impedes accurate quantification of tracer accumulation in small tissue components. Low resolution leads to image blurring by displacement and mixing of signals from adjoining sources, thus obscuring the tracer distribution profile in tissues [1]. For example, the accumulation profile of 18-Fluorodeoxyglucose (FDG) in arterial tissues has been the subject of longstanding debate [2], however, *in vivo* quantification of the activity contribution of arterial wall components has not been possible, due to the limited resolution of PET. Another limitation of PET is that current scanning and quantification techniques do not provide a framework for quantitative assessment of factors affecting tracer uptake. For example, hypoxia is known to enhance tissue FDG uptake [3], but *in vivo* quantification of the strength of this effect under various conditions is not readily supported by current PET techniques.

In this paper, we aim to mitigate the above limitations by using quantification methods based on modelling of the PET signal. The principle is to 1) construct a model describing all signal components either as linear or non-linear superposition 2) incorporate information into the model from PET scans and also from other sources, e.g. data from histology or data from other scan modalities and 3) use regression analyses to estimate any unknown parameters in the model. In this paper, we use *in silico* simulations to provide examples of the quantitative applications of signal modelling, and we use phantom scans to validate our simulation algorithm. First, we provide simulations of tumors with hypoxia, as an example of how signal mod-

eling may help quantify the effect of biological mechanisms on tracer accumulation. Furthermore, we present vascular scan simulations showing that signal modelling may facilitate accurate quantification of the activity fraction of sub-resolution tissue components. The modelling approach presented here is not restricted to the provided examples but may be applicable in PET imaging in general. The presented concept may, thus, contribute to the development of PET as a quantitative tool for characterization and monitoring of physiological and disease processes.

Methods

General model of PET signal

The aim of this study was to develop a quantification approach based on signal modelling to extend the quantitative utility of PET imaging. The total activity (A) measured in a region of interest (ROI) is the sum of a) activities originating from sources within the ROI, and b) signal displacement effects, also known as partial volume effects, across the ROI borders. The total signal can thus be described as:

Eqn. 1

$$A_{ROI} = A_t + A_{nt} - A_l + A_g$$

Where A_t is total activity of target tissue/structure, A_{nt} is activity of non-target (i.e. background) structures, A_l is total activity displaced and lost outside the ROI due to signal displacement, and A_g is activity gained in the ROI from the outside due to signal displacement. Based on Eqn. 1, we derived models for specific applications as detailed in the **Appendix** and summarized in the following sections.

Modelling of factors affecting tissue tracer accumulation

We derived a model to describe situations where multiple tissue properties or tissue-related factors may interact with each other and modify tracer uptake. Derivations of the full model are presented in the **Appendix** (Eqn. S4). An example of such interaction is the effect of hypoxia on the accumulation of a metabolic tracer, e.g. the glucose analogue FDG. Hypoxia is known to enhance tissue glucose turnover and, thus, augment FDG uptake [3]. Using *in silico* simulations, we aimed to illustrate the use of the modeling approach to separate the tissues' "basal" level of FDG accumulation under non-hypoxic conditions from the augmented level of accumulation resulting from hypoxia. Based on Eqn. S4, we derived the following model, where hypoxia interacts with tissue volume/cellularity to augment tracer uptake:

Eqn. 2

$$A_{ROI} = C_t \cdot V_t + I \cdot L_h \cdot V_t - A_l + A_g$$

Where V_t is volume of viable (non-necrotic) tumor tissue, C_t is the basal tissue activity concentration under non-hypoxic conditions, L_h is the level of hypoxia and I is the level of interaction.

Computer simulations of tumors

We aimed to produce simulations of tumors that were as realistic as possible: 1) the tumors were simulated with randomly varied irregular shape and with heterogeneous activity, including necrotic regions (**Figure 1**), 2) the background was also simulated to be heterogeneous, 3) random noise was introduced in target and background, and 4) variability was introduced in the full width half maximum (FWHM) of the point spread function (PSF) to simulate differences in imaging systems and spatial PSF variance. To simulate realistic quantification of these *in silico* tumors, 5) uncertainty was introduced in ROI delineation in the computer simulations.

As detailed in the **Appendix**, the heterogeneous activity concentrations in tumor and background were set according to values from human scans. Each tumor was assigned a level of hypoxia (L_h), randomly drawn from a range of 0-10 (arbitrary scale). Hypoxia is not itself a site of tracer accumulation, but it may modify the tissues' tracer avidity [3]. Therefore, the effect of hypoxia was introduced in the simulations as an interaction (I) that was randomly drawn from a normal distribution with mean of 5 and standard deviation (SD) of 0.5 (arbitrary units, a.u.). The product of the level of hypoxia multiplied by the interaction term ($L_h \times I$), represented the magnitude of tracer uptake that was induced by hypoxia. This product was therefore added to all voxels in the viable part of the simulated

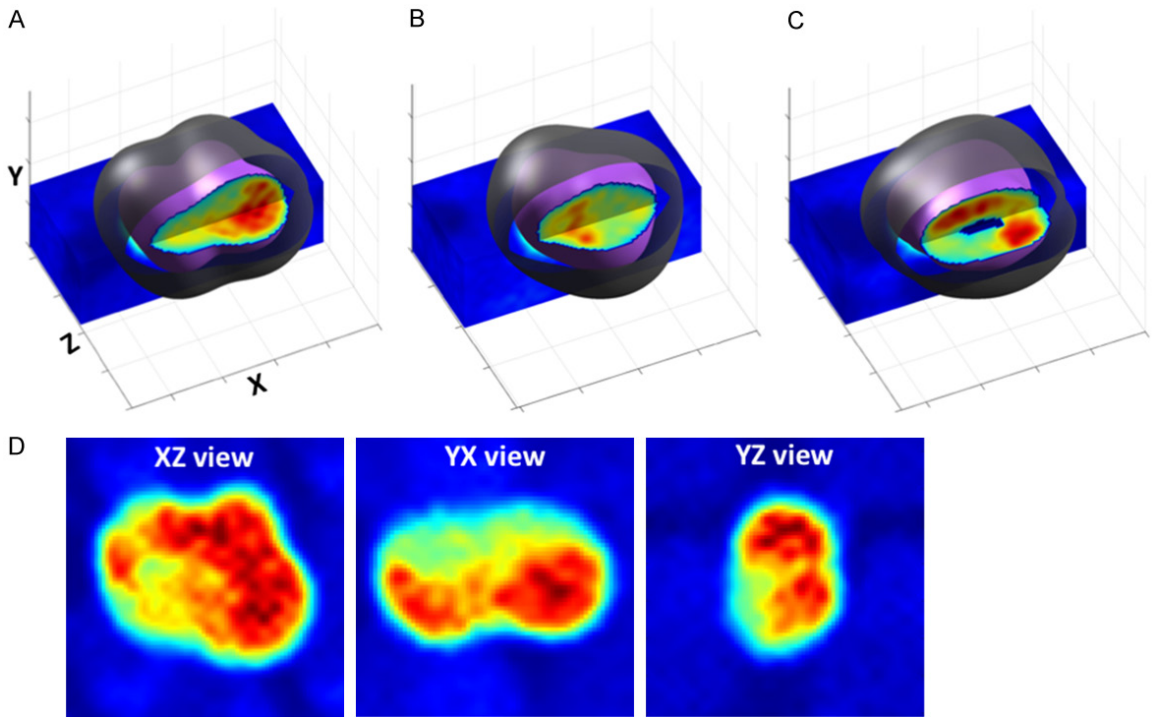

Figure 1. Examples of *in silico* simulated tumors. (A-C) Three examples of tumors produced using the algorithm for generation of smooth-surface randomly-variable irregular shapes. Cutaways are shown allowing to visualize the inside of the high-activity tumors and the low-activity background. Linear rainbow color-coding is used to represent activity concentration, with red representing the highest value. Tumor surface (purple) and expanded region of interest (dark envelope) are colored separately for demonstration. A central necrotic region is seen in (C). (D) Orthogonal reformatted slices/views through the center of (A).

tumor (necrotic region voxels were left at zero activity concentration). Thus, the tumors were simulated to contain a "basal" level of heterogeneous activity and an additional level of activity induced by hypoxia.

"Ground truth" images of the tumors were constructed as outlined above. Binary volumes representing tumor edges (edge mask) were generated based on the ground truth images to simulate anatomical reference images. Subsequently, the ground truth images were converted into simulated PET images by 1) convolution with a 3D Gaussian PSF and 2) resampling at 2 mm/voxel. The FWHM of the PSF was drawn randomly in the range of 6-8 mm, corresponding to the FWHM of clinical PET scanners [4]. Finally, a relatively high level of noise was added to the signal to achieve a noise to signal ratio (NSR) of 10%.

Quantification of signal from simulated tumors

The conventional method for quantification of a target's signal is to delineate a ROI fitting the target, either using anatomical images or thresholding directly on the PET images. We refer to such ROIs as "regular ROIs". Regular ROIs may not recover the correct target signal due to signal displacement effect, as previously reported [1]. Signal displacement is the result of 1) the cumulative PSF of the imaging system, 2) a finite spatial sampling, i.e. reconstruction voxel volume (**Figure 2**) and 3) imperfect image corrections for scattering, attenuation etc. The cumulative PSF, often approximated by a Gaussian function, is the combined effect of a number of factors, including physical properties such as positron annihilation range, hardware attributes such as detector size/geometry, and data processing effects such as post-reconstruction noise filtering. To achieve full signal recovery, an expanded ROI that protrudes outside the target lesion can be used, as previously described [5-7]. By expanding the ROI to protrude at least 1.25 × FWHM of the PSF outside the target's anatomical borders, net signal displacement around the new ROI border is essentially abolished. This is because 1) for a Gaussian PSF, ROIs protruding 1.25 ×

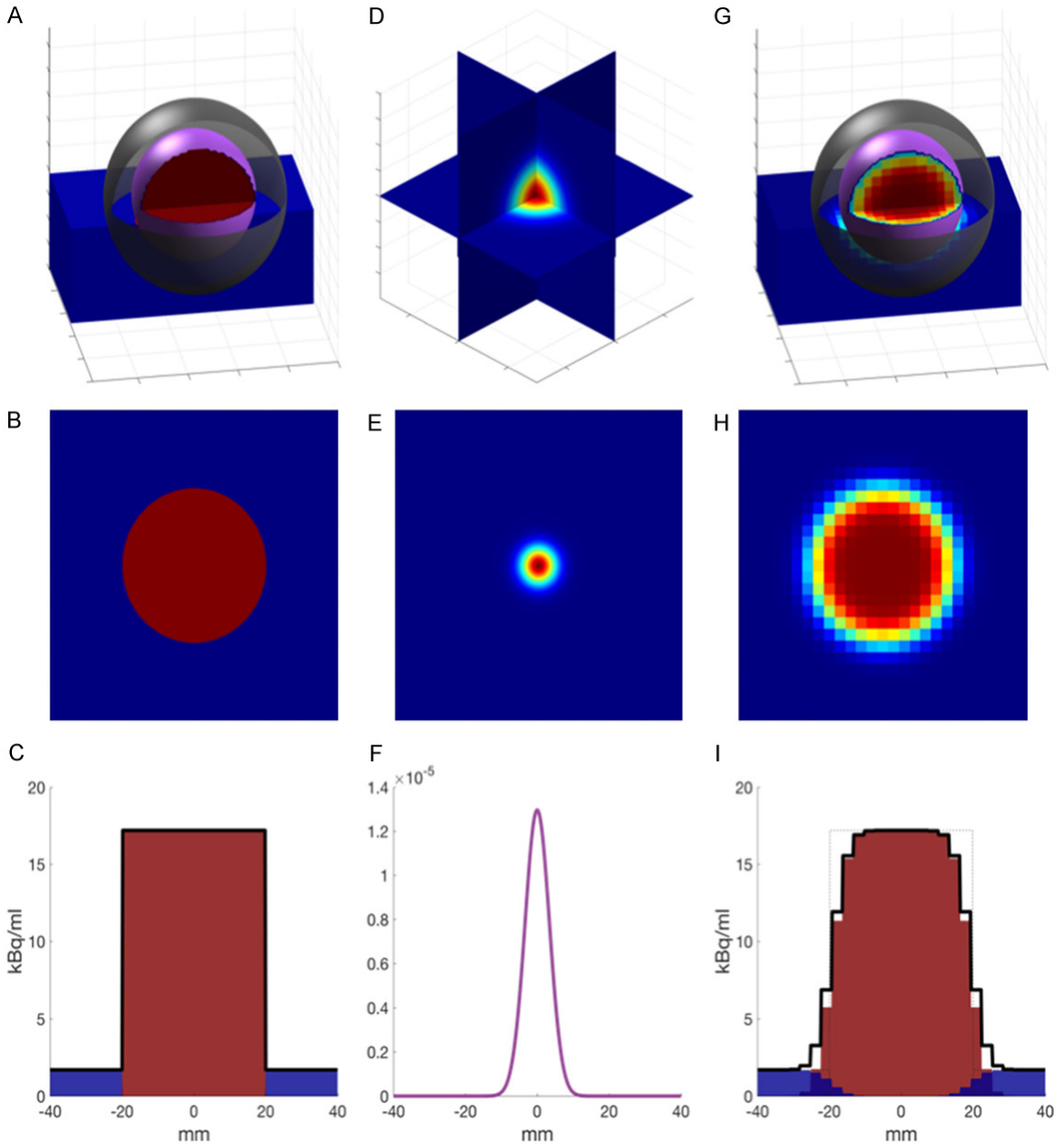

Figure 2. Computer simulations of scans of the NEMA phantom spheres. (A) 3D cutaway illustration of the ground truth simulation of a spherical phantom. Linear rainbow color-coding is used to represent activity concentration, with red representing the highest value. Sphere surface (purple) and expanded region of interest (dark envelope) are colored separately for demonstration. (B, C) A slice and a linear profile, respectively, through the center of the ground truth volume presented in (A). (D-F) A Gaussian point spread function used as the convolution filter. (G-I) The simulated PET volume (G) slice (H) and linear profile (I) showing signal displacement as the result of convolution and resampling. Target (red) and background (blue) are colored differently for illustration. The linear profile in (I) illustrates signal displacement from the sphere and the background outside their original locations. The magnitude of the total signal (area under the solid line) is equal in (C) and (I) and is, thus, preserved through convolution and resampling.

FWHM will contain at least 99.7% of all the signal originating from within the target and, thus, virtually no signal from the target will be displaced far enough to pass the expanded ROI and 2) the new ROI border will be flanked by background structures on both sides, and net signal displacement across the border will be, on average, approximately zero (**Figure 2**). Thus, the parameters A_l and A_g cancel out in Eqn. 2. The validity of using expanded ROIs for full

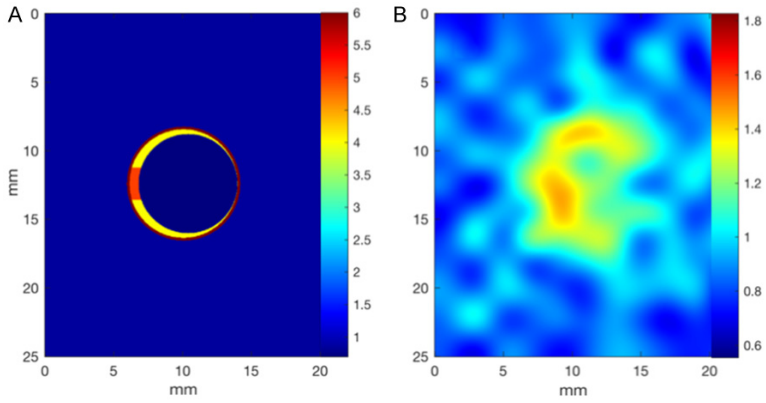

Figure 3. Example of an arterial scan simulation. (A) Simulated ground truth artery wall containing a circular tunica media, a crescent-shaped thickening of the tunica intima (atherosclerotic plaque) and a collection of macrophages. (B) The simulated PET image generated by point spread function convolution and resampling (2 mm/pixel) of (A) and with added noise. Color-coding is in concordance with displayed scale (standardized uptake value).

tumor signal recovery has been shown in several previous studies [5-7]. Using expanded ROIs, the signal model describing tumor hypoxia becomes:

Eqn. 3

$$A_{expROI} = C_t \cdot V_t + I \cdot L_h \cdot V_t + C_{nt} \cdot V_{nt}$$

Where A_{expROI} is the total activity in the expanded ROI, C_{nt} is the activity concentration of non-target (background) structures contained within the expanded ROI, and V_{nt} in the volume of non-target structures in the expanded ROI.

The regular ROIs were adjusted to tumor boundaries using the edge mask, simulating tumor delineation using anatomical reference images, e.g. computed tomography (CT) scans. The expanded ROIs were drawn by expanding the regular ROIs 10 mm outwards. Errors were introduced in tumor delineation, and thereby in delineation of expanded ROIs to simulate delineation uncertainty on anatomic scans. This uncertainty in ROI delineation was based on variability reported in human tumor delineation, as detailed in the **Appendix**.

The A_{expROI} was measured directly in the simulations. Volume of the viable part of tumor (V_t) was recorded as tumor volume minus necrosis volume. The level of hypoxia (L_h) was simulated to be available from a separate source (e.g. PET scan with a hypoxia tracer [8]) and quantified with uncertainty (error SD of 10%). Volume of background contained within the expanded ROI (V_{nt}) was calculated as the difference between the volume of the expanded ROI and the volume of the target. Background activity concentration (C_{nt}) was measured in a 2-voxel thick shell around the surface of the expanded ROI. Finally, the above measurements were entered in multivariable regression analysis to estimate averages of the non-hypoxic tracer activity concentration (C_{nt}) and the effect of hypoxia on tracer accumulation (I). More details regarding the simulation parameters are provided in the **Appendix**.

Computer simulations of vascular PET scans

Simulations of vascular PET were conducted to illustrate the utility of signal modelling in estimating the relative contribution of sub-resolution small tissue components to the total artery PET signal. PET images were generated *in silico* to simulate iliac vessels. The artery wall comprised a circular tunica media and a crescent-shaped atherosclerotic plaque containing a collection of macrophages (**Figure 3**). Activity concentrations of blood and background, in addition to dimensions of vessels' lumina and wall components, were based on previously published data from *in vivo PET* scans [9] and histopathology [9, 10] of atherosclerotic minipig iliac arteries.

Two scenarios were simulated regarding activity concentrations in the artery wall. Scenario 1: the activity concentration of all arterial tissue components was set to 5±1.7 g/cm^3. This value was chosen, because it resulted in mean and max values, following convolution and resampling, that were similar to values measured *in vivo* [9]. Scenario 2: the macrophage activity concentration was increased five-fold to simulate macrophages being dominant in tracer accumulation. Regular circular ROIs, with uncertainty in delineation, were placed around each vessel section (i.e. expanded ROIs extending 1.25 FWHM were not used). The simulations were carried out with the use of regular ROIs because we only aimed to quantify the *relative* contribution of the arterial components

Table 1. *Monte Carlo* computer simulations of hypoxia in tumors

Parameter	Assigned	Estimated by regression	Unit
C	7.9±1.0	8.0±0.2	g/cm^3
I	5.0±0.5	5.0±0.1	a.u.

One thousand simulations were conducted of tumors with variable levels of hypoxia. C: average activity concentration in tumors in the absence of hypoxia. I: the interaction term signifying the effect of hypoxia on tissue tracer avidity. a.u.: arbitrary units. Assigned values are mean ± standard deviation. Estimated regression coefficients are shown ± standard error.

to the signal, although an equivalent approach based on expanded ROIs could also be derived. This application also demonstrated the utility of signal modelling in cases where expanded ROIs are not required or impractical.

For each of the two scenarios mentioned above, 100 sets of simulations were generated, each comprising 100 simulated vessels. Data from each vessel was entered into the regression as a single observation. Following each set of simulations, multi-variable regression analysis was conducted yielding *estimated* activity concentrations in the arterial components. The regression equation was derived based on the signal model, as detailed in the **Appendix** (Eqn. S17):

Eqn. 4:

$$A_{ROI} = \sum_{i=1}^{3} (C_{ai}^{o} \cdot V_{ai}) + \bar{C}_v \cdot V_{ROI}$$

Where A_{ROI} is total activity measured in the arterial ROI, V_{ROI} is the volume of the arterial ROI, $C_{a1..a3}^{o}$ are the estimated regression coefficients denoting activity concentrations of the arterial tissues (macrophages, intima and media), $V_{a1..a3}$ are volumes of the tissues, and $\bar{C}_v$ is the average activity concentration measured in the reference vein. The tissue volumes were simulated to be known, e.g. from histopathology.

The *activity fraction* (AF) was defined as the relative contribution of each tissue component to the total activity of the entire arterial wall. The *assigned* AF was calculated using tissue volumes and assigned tissue activity concentrations in concordance with Eqn. S18 in the **Appendix**. An *estimated* AF was calculated similarly, except using activity concentrations estimated by the regression analysis, i.e. using Eqn. S19 in the **Appendix**.

Phantom scans

A National Electrical Manufacturers Association (NEMA) Image quality phantom (NEMA 2012 body phantom) was prepared following the European Association of Nuclear Medicine's procedure for FDG-PET/CT accreditation (EARL) [11], as detailed in the **Appendix**. Regular and expanded spherical ROIs were used to quantify the activity in each sphere. Background activity concentration was measured in a 2-mm thick shell around the surface of the expanded ROI. The signal recovery fraction was calculated as the *measured* activity concentration divided by the *true* activity concentration. A hot sphere NSR was measured within a 15 mm in diameter central ROI in the largest sphere, yielding a value of 2.3%. Further procedural details are provided in the **Appendix**.

Computer simulations of the NEMA phantom PET scans

The phantom scan experiment outlined in the above was replicated *in silico* in order to validate the simulation algorithms. "Ground truth" images of high-activity spheres surrounded by low-activity background were simulated (**Figure 2**). The diameters of the simulated spheres corresponded to diameters of the NEMA phantom. Sphere and background activity concentrations were set to be homogenous and equal to the known activity concentrations in the actual PET scans. Binary volumes representing sphere edges were created as described above. The ground truth images were converted into simulated PET images using steps similar to the tumor simulations. Measurements were simulated using regular and expanded ROIs. Background activity concentrations were recorded as the average value in a 2-voxel wide shell around the surface of the expanded ROIs. To investigate the effect of noise, three computer simulations of the phantom scans were conducted, adding noise with NSR values of 0%, 2.3% (corresponding to actual PET scans) and 10%, respectively.

Statistical analyses

Regression analyses were conducted using Stata 15 (StatCorp, USA). Linear regression was used to analyze vascular scan simulation results. Tumor hypoxia scans were simulated with multiplicative errors and, therefore, Eqn. 3

Table 2. *Monte Carlo* computer simulations of vascular PET scans

	Activity concentration (g/cm³)		Activity fraction (%)	
	Assigned	Estimated by regression	Assigned	Estimated by regression
Scenario 1: assigned activity concentrations equal in all tissues				
Mφ	5.0±1.7	2.3±0.2	16.5±7.4	16.9±1.1
Intima	5.0±1.7	2.2±0.1	45.5±12.9	45.3±1.5
Media	5.0±1.7	2.2±0.1	38.0±13.0	37.9±1.0
Scenario 2: assigned activity concentration highest in macrophages				
Mφ	25.0±8.3	13.1±0.3	47.1±12.9	49.6±1.0
Intima	5.0±1.7	2.4±0.1	28.7±10.2	25.7±1.1
Media	5.0±1.7	2.7±0.1	24.2±10.1	24.8±0.8

In each scenario, 100 sets of simulations were conducted, each set comprising 100 simulated vessels. The activity fractions were calculated as the activity of each tissue component in percentages of the total activity of the entire artery wall. Intima signifies non-macrophage part of the intima. Mφ: macrophages. Assigned values are mean ± standard deviation. Estimated regression coefficients are presented as mean ± standard error of the mean.

was logarithmically transformed in order to transform the errors to additive form, and then non-linear regression was conducted.

Results

Investigating biological mechanisms affecting tissue tracer accumulation

We aimed to demonstrate the utility of signal modelling in quantitative assessment of mechanisms affecting tracer uptake, here exemplified by the effect of hypoxia on the uptake of a metabolic tracer like FDG in tumors. The tumor simulations were constructed to be as realistic as possible by assigning variable shapes to tumors and using heterogonous and noisy signals for tumor and background (**Figure 1**). The average standardized activity concentration assigned to the tumors was 7.9±1.0 g/cm³. In addition, each tumor was assigned a random level of hypoxia, with an average of 5.0±0.5 a.u.. The quantifications were conducted using expanded ROIs that had uncertainty introduced in size and location, to simulate uncertainty in ROI delineation of actual scans. A measure of hypoxia, quantified with uncertainty, was simulated to be available from a separate source. Regression analyses based on Eqn. 3 enabled accurate extraction of the average non-hypoxic basal tracer accumulation, yielding 8.0±0.2 g/cm³. Similarly, the effect of hypoxia on tracer uptake was accurately estimated at 5.0±0.1 a.u. (**Table 1**).

Quantification of activity fractions of sub-resolution tissue components

Using vascular PET scans as an example, we aimed to demonstrate how signal modelling can be used for quantification of the relative contribution of various tissue sub-compartments to total tissue activity, i.e. each tissue's activity fraction.

In silico simulations of vascular PET scans were conducted using data from actual PET scans and histopathological analysis of atherosclerotic minipig vessels [9, 10]. The dimensions of the simulated artery wall and its components were approximately an order of magnitude smaller than the simulated scan resolution (FWHM 6-8 mm) (**Figure 3**).

Using regression analysis based on Eqn. 4, estimated activity concentrations were obtained for the arterial tissue types. As detailed in the derivations of the model (**Appendix**), the estimated activity concentrations were expected to be lower than the assigned tissue activity concentrations (**Table 2**), due to the use of regular ROIs (i.e. not expanded ROIs) that do not provide full signal recovery. However, the signal recovery was similar for all tissues, and, importantly, the estimated activity fractions were, thus, predicted with high accuracy, within an error margin of approximately 3% points (**Table 2**).

Phantom scans

Scans of a standardized PET phantom were conducted and the results were compared with *in silico* simulations of the phantom, in order to investigate the validity of our simulation algorithm. Using regular ROIs to enclose a target structure yields incomplete and volume-dependent signal recovery, due to signal displacement, as previously reported [1]. We illustrated this on an actual PET scan of the NEMA Image Quality phantom and the observations were perfectly reproduced by our computer simulations using regular ROIs (**Figure 4A**). The ROI max activity concentration scaled with volume and was, furthermore, burdened by noise-

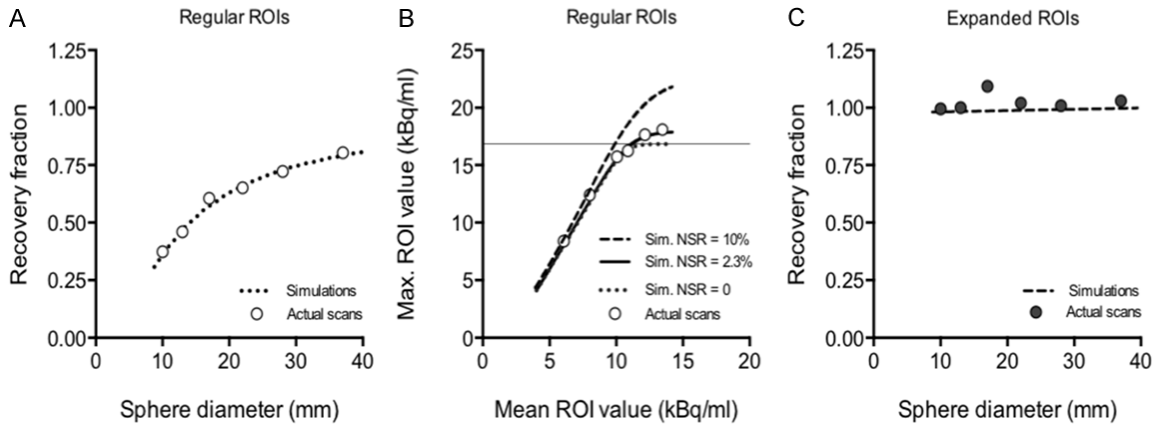

Figure 4. Computer simulations and actual PET scans of the NEMA body phantom. (A) Signal recovery fractions obtained from actual PET scans and *in silico* scan simulations using regular regions of interest (ROI) adjusted to phantom sphere borders. (B) The determinants of ROI max value using the regular ROIs. The noise to signal ratio (NSR) in the actual PET scans was 2.3%. All phantom spheres contained a solution with the same activity concentration (horizontal line). Best-fit curves of 3 computer simulations are shown with different NSR levels, as indicated. (C) Recovery fractions obtained from actual PET scans and *in silico* scan simulations using expanded ROIs. All *in silico* simulation parameters were based on the actual PET scans of the NEMA phantom.

dependent bias, which was also in full agreement with the results of our simulations (**Figure 4B**). Using expanded ROIs, the recovery fractions were close to 100% for all spheres, and this was also fully reproduced in our computer simulations (**Figure 4C**).

Discussion

One of the main limitations of PET is the low resolution of clinical systems, leading to signal displacement effects, also known as partial volume effects. The spatial resolution of an image is the smallest distance at which two points can be differentiated and is generally considered to be equivalent to the FWHM of the PSF. The cumulative PSF of a PET imaging system arises from multiple factors that amount approximately to a Gaussian function with a FWHM of approximately 6-8 mm for clinical scanners [4]. In addition, signal displacement is further exacerbated by large voxel volumes, often used in PET image reconstruction [1]. Collectively, these effects compromise the quantitative utility of PET imaging in many important areas. One example is encountered in imaging of sub-resolution arterial tissues, where signal displacement distorts tissue tracer distribution, hampering direct quantification of the activity fraction of tissue sub-compartments.

Another limitation of PET is that tracer accumulation in tissues may be affected by multiple factors that may vary between subjects and between scans, causing variability in the obtained imaging results. Although the influence of a number of these factors such as hypoxia, perfusion and inflammation on tracer uptake has been studied extensively, accurate quantification of the magnitude of their modificatory effects using PET imaging is not readily supported by current methods.

In this paper, we present quantification methods based on signal modelling that may alleviate the limitations mentioned above, potentially improving and expanding the quantitative capacity of PET. Using computer simulations, we show how signal modelling may unveil the activity fraction of sub-resolution small tissues and quantify the effect of different mechanisms on tissue tracer uptake. We exemplify our approach in the context of cancer and vascular imaging, but the presented methodology may be useful in other areas of PET imaging as well.

Separating signal sources

Our modelling approach can be used to investigate various tissue properties and their impact on tracer accumulation. We exemplified this application in two contexts, both incorporating supplemental information available either from another imaging technique (e.g. another PET-tracer) or from subsequent histopathology.

As an example of the first type, we simulated tumor hypoxia, which is known to enhance FDG accumulation [3]. We simulated random tumors with varying levels of hypoxia, graded on an arbitrary scale. The contribution of hypoxia to the FDG signal was treated as an interaction, describing the strength of the hypoxia-induced enhancement. Using regression analysis, both the non-hypoxic tissue concentration and the hypoxia interaction terms could be extracted at high accuracy (**Table 1**). We exemplified this application in the context of tumor hypoxia, but similar applications studying the effect of perfusion, inflammation and necrosis on tracer uptake are conceivable.

As an example of the second type, we simulated vascular FDG-PET scans. Quantification of the distribution pattern of specific tracers in tissue sub-compartments is important in many areas of nuclear imaging. For instance in vascular PET, great effort has been invested in quantification of the relative activity of arterial wall tissues, specifically atherosclerotic plaque macrophages, which are proposed to be the dominant site of FDG accumulation in arteries [2]. However, conventional approaches do not support direct *in vivo* quantification of the activity fraction of macrophages. Quantification based on signal modelling revealed the activity fraction of sub-resolution arterial structures with high accuracy, even though the tissues were simulated to be an order of magnitude smaller in dimensions compared with scan resolution. For demonstration, we derived the equations based on regular ROIs to address this issue, although alternative equations based on expanded ROIs could also be used.

Limitations

The presented results in this paper are mainly based on *in silico* simulations and the validity of the results, therefore, depends on the validity of the simulation algorithm, including the simulation parameters. It is a fundamental limitation in PET research that studies similar to ours lack a gold-standard approach for verification [6] and *in silico* simulations and phantom scans are often used in the field to introduce new methods and concepts.

We aimed to make the simulations as realistic as possible by attempting to replicate the shape of atherosclerotic arteries and the irregular and variable shapes of tumors. Furthermore, we used activity concentrations of target and background that were based on values from human and animal scans. In addition, to simulate measurement uncertainty of real data, we introduced measurement errors in all measurements, e.g. errors in ROI delineation, level of hypoxia etc. Finally, we validated our simulation algorithm against actual PET scans of phantoms and found almost perfect agreement. Nevertheless, the concepts and methodology introduced in this paper need further evaluation and verification in future experiments.

Conclusion

We present the concept of PET signal modelling that may be used as a general framework for analysis of PET images. Using *in silico* simulations, we demonstrate applications for the approach not supported by current methods, such as estimating activity fractions of sub-resolution tissues and probing the effect of different biological properties on tracer avidity. The methods presented here are easy to adapt and implement in a clinical setting and do not require changes in scan protocols. The modelling approach is not restricted to the examples provided in this paper but may provide a general framework for image quantification that may improve and expand the quantitative accuracy of PET imaging in research and clinical practice.

Acknowledgements

This work was supported by the Danish Heart Foundation.

Disclosure of conflict of interest

None.

Author contributions

RHA conceived the signal modeling approach and derived the equations. RHA programmed the *in silico* simulations. LPT conducted the phantom scans. RHA conducted all data analyses. All authors critically revised and approved the manuscript.

Address correspondence to: Dr. Rozh H Al-Mashhadi, Department of Radiology, Aarhus University Hospital, Aarhus, Denmark. E-mail: rham@clin.au.dk

References

[1] Soret M, Bacharach SL, Buvat I. Partial-volume effect in PET tumor imaging. J Nucl Med 2007; 48: 932-45.

[2] Sheikine Y, Akram K. FDG-PET imaging of atherosclerosis: do we know what we see? Atherosclerosis 2010; 211: 371-80.

[3] Dierckx RA, Van de Wiele C. FDG uptake, a surrogate of tumour hypoxia? Eur J Nucl Med Mol Imaging 2008; 35: 1544-9.

[4] Ikari Y, Akamatsu G, Nishio T, Ishii K, Ito K, Iwatsubo T, Senda M. Phantom criteria for qualification of brain FDG and amyloid PET across different cameras. EJNMMI Phys 2016; 3: 23.

[5] Hickeson M, Yun M, Matthies A, Zhuang H, Adam LE, Lacorte L, Alavi A. Use of a corrected standardized uptake value based on the lesion size on CT permits accurate characterization of lung nodules on FDG-PET. Eur J Nucl Med Mol Imaging 2002; 29: 1639-47.

[6] Hofheinz F, Langner J, Petr J, Beuthien-Baumann B, Oehme L, Steinbach J, Kotzerke J, van den Hoff J. A method for model-free partial volume correction in oncological PET. EJNMMI Res 2012; 2: 16.

[7] Bundschuh RA, Essler M, Dinges J, Berchtenbreiter C, Mariss J, Martínez-Möller A, Delso G, Hohberg M, Nekolla SG, Schulz D, Ziegler SI, Schwaiger M. Semiautomatic algorithm for lymph node analysis corrected for partial volume effects in combined positron emission tomography-computed tomography. Mol Imaging 2010; 9: 319-28.

[8] Sun X, Niu G, Chan N, Shen B, Chen X. Tumor hypoxia imaging. Mol Imaging Biol 2011; 13: 399-410.

[9] Al-Mashhadi RH, Sørensen CB, Kragh PM, Christoffersen C, Mortensen MB, Tolbod LP, Thim T, Du Y, Li J, Liu Y, Moldt B, Schmidt M, Vajta G, Larsen T, Purup S, Bolund L, Nielsen LB, Callesen H, Falk E, Mikkelsen JG, Bentzon JF. Familial hypercholesterolemia and atherosclerosis in cloned minipigs created by DNA transposition of a human PCSK9 gain-of-function mutant. Sci Transl Med 2013; 5: 166ra1.

[10] Al-Mashhadi RH, Bjørklund MM, Mortensen MB, Christoffersen C, Larsen T, Falk E, Bentzon JF. Diabetes with poor glycaemic control does not promote atherosclerosis in genetically modified hypercholesterolaemic minipigs. Diabetologia 2015; 58: 1926-36.

[11] Boellaard R, Willemsen AT, Arends B, Visser EP. EARL procedure for assessing PET/CT system specific patient FDG activity preparations for quantitative FDG PET/CT studies. eanm.org. 2013; 1-3.

Appendix

Supplemental methods

Computer simulations of tumors

A ground-truth volume was simulated to contain tumors that were modelled with a smooth-surface but irregular (non-spherical) shapes to resemble real tumors. The volume of simulated lesions was drawn randomly within the range of 2-100 cm^3 using a random numbers generator. The tumors were simulated to contain patches of inhomogeneous activity with the activity concentration in each patch randomly chosen from a range of 5-11 g/ml, corresponding to typical standardized uptake values (SUVs) measured on positron emission tomography (PET) scans using 18-Fluorodeoxyglucose (FDG) in human colorectal liver metastases (SUV of approximately 5 g/ml) and lung cancer (SUV of approximately 11 g/ml) [1, 2]. These patches were also of random shape and position and had a random volume of up to 20 cm^3. In addition, the tumors were simulated with a central necrosis, containing zero activity. The necrosis volume was randomly drawn between 0 cm^3 and up to a volume allowing at least a 5-mm thick rim of non-necrotic tissue in each tumor. The background healthy tissue activity concentration was also simulated to be patchy, i.e. heterogeneous. The activity concentration of each background patch was randomly set to 0.5-2 g/ml corresponding to values measured in normal human lung (SUV of approximately 0.5 g/ml) and liver (SUV of approximately 2 g/ml) tissues [2, 3].

Errors in region of interest (ROI) volume and position were introduced in all ROIs to simulate uncertainty in tumor delineation. First, ROI size was multiplied by a random error factor that was drawn from a normal distribution with mean of 1 and a standard deviation (SD) of 15%. This produced random variation in the ROI size with a 95% prediction interval (PI95) of approximately 70%-130%. A 15% SD for the ROI size error was chosen in concordance with variability reported previously in measurements of human tumor volumes on computed tomography (CT) images [4, 5]. Second, the position of each ROI was randomly shifted along all three dimensions with an SD of 2 mm in each direction, producing a total ROI position PI95 displacement error of ±6.8 mm.

Computer simulations of vascular PET scans

For the ground-truth images, arteries and veins were simulated with a luminal radius drawn randomly from distributions with mean and variation similar to those measured on CT angiograms of minipig iliac vessels. Each vessel was simulated to span 10 PET slices. The volumes of the arterial components were drawn randomly from distributions with mean and variation similar to those measured on tissue micrographs of minipig ilio-femoral arteries [6, 7]. The vein was simulated in close proximity to the artery. Because veins have very thin walls, vein wall tissue was considered negligible. The simulated activity concentration of blood in the lumen of arteries and veins was drawn randomly from a distribution reflecting average activity concentration that was measured at the center of iliac veins on *in vivo* PET scans of minipigs [7]. Background activity concentration outside the vessels was drawn randomly for each imaging slice from a distribution reflecting activity concentration measured in a 6 cm^2 large ROI around the iliac vessel on the *in-vivo* PET scans.

The ground truth images were convolved by a Gaussian point spread function (PSF) with a full-width half maximum (FWHM) randomly selected within a range of 6-8 mm and resampled at 2 mm/pixel. Noise was added to the signal to achieve an noise to signal ratio (NSR) of 10%.

A random error with an SD of ±10% was introduced into the size of the ROI, leading to a variation with a PI95 of approximately 80%-120%. In addition, the position of the ROI was randomly shifted along the two in-plane dimensions with an SD of 1 mm, leading to a total ROI positional displacement error with a PI95 of ±2.8 in a random direction in-plane.

Phantom scans

A National Electrical Manufacturers Association (NEMA) Image quality phantom was prepared. The cylinder of the phantom was filled with an FDG solution with an activity concentration of 1.7 kBq/ml at time

of scan and the 6 spheres were filled with a 10 times higher concentration. The spheres were 10, 13, 17, 22, 28 and 37 mm in inner diameter. The phantom was scanned on a GE Discovery MI Digital Ready PET/CT (Discovery 690; GE Healthcare). An initial CT scan was used for localization and attenuation correction. PET images were acquired using two bed positions, each with a duration of 10 minutes. PET images were reconstructed at a resolution of 2.73 × 2.73 × 3.27 mm using the VuePoint FX algorithm (2 iterations, 24 subsets, 7 mm 2D Gaussian post-filter in transaxial plane and a 3-point convolution post-filter [1 2 1] in the axial direction).

Signal model derivations

A general model of positron emission tomography signal

Based on the superposition principle, the total signal within a finite volume (V) of a ROI is a linear combination of signals from all sources within the ROI. In addition, due to the PSF of the imaging system and finite spatial sampling, considerable signal displacement may also be present, where some signal originating inside the ROI may be dispersed to outside the ROI and *vice versa*. The total signal can, therefore, be described as:

Eqn. S1

$$A_{ROI} = A_t + A_{nt} - A_l + A_g$$

- A_{ROI} total activity (A) in the ROI
- A_t total activity of target structures within the ROI
- A_{nt} total activity of non-target structures within the ROI
- A_l lost activity (from all ROI structures), due to signal displacement
- A_g gained activity from surroundings, due to signal displacement

The contribution of possible multiple target tissues or different sub-compartments in the target tissue can be expressed by including separate terms for each target tissue component:

Eqn. S2:

$$A_{ROI} = \sum_{i=1}^{n} (A_{ti}) + A_{nt} - A_l + A_g$$

- $A_{t1..tn}$ activity of target tissues types 1..n

The activities may be expressed in terms of volumes and activity concentrations:

Eqn. S3

$$A_{ROI} = C_{ROI} \cdot V_{ROI} = \sum_{i=1}^{n} (C_{ti} \cdot V_{ti}) + C_{nt} \cdot V_{nt} - A_l + A_g$$

- C_{ROI} mean activity concentration (C) in the ROI
- V_{ROI} volume of the ROI
- $C_{t1..tn}$ activity concentration in target tissue types 1..n
- $V_{t1..tn}$ volume of target tissue types 1..n
- C_{nt} mean activity concentration of non-target structures in the ROI
- V_{nt} volume of non-target structures in the ROI

Total activities are measured in Bq. Volumes are measured in cm^3 (or ml) and activity concentrations are measured in Bq/cm^3 or (Bq/ml). The activity and activity concentration may be standardized to injected tracer dose (Bq) and body weight (g) to get SUVs. The standardized total activities are measured in g and standardized activity concentrations are measured in g/ml.

Modelling interactions

In certain cases, tissue properties that determine the signal are not merely additive, but may interact with each other. To describe signal generated via such interactions, the model may be expanded to include interactions of pairs of tissue properties:

Eqn. S4

$$A_{ROI} = \sum_{i=1}^{n} (C_{ti} \cdot V_{ti}) + \sum_{j=1}^{m} (I_j \cdot P_{xj} \cdot P_{yj}) + C_{nt} \cdot V_{nt} - A_l + A_g$$

- $I_{1..m}$ interaction coefficients for interactions 1..m
- P_{xj} property xj of target tissue
- P_{yj} property yj of target tissue

Application of the general model to vascular PET

Considering vascular PET, where ROIs are adjusted to encompass the vessel, total activity in a ROI encompassing a *vein* can be described as:

Eqn. S5:

$$A_{ROI} = A_b - A_{lb} + A_g$$

- A_b activity of lumen/blood
- A_{lb} lost activity from blood due to signal displacement outside the ROI

The vein wall is considered of negligible volume and contribution to the signal. The activities can be expressed in terms of volumes and activity concentrations:

Eqn. S6:

$$\overline{C}_v \cdot V_v = C_b \cdot V_v - \overline{C}_{lb} \cdot V_v + \overline{C}_g \cdot V_v \Longleftrightarrow \overline{C}_v = C_b - \overline{C}_{lb} + \overline{C}_g$$

- V_v total vein volume (this is equivalent to the ROI volume)
- $\overline{C}_v$ vein activity concentration (averaged for the entire vein volume, i.e. ROI volume)
- C_b activity concentration of blood
- $\overline{C}_{lb}$ activity concentration lost from ROI due to displacement (mean of entire ROI)
- $\overline{C}_g$ activity concentration gained in the ROI due to displacement (mean of entire ROI)

Considering the artery wall as the target structure and the blood in its lumen as background (non-target structure), the *arterial* PET signal can be expressed as:

Eqn. S7:

$$A_{ROI} = A_a + A_b - A_l + A_g$$

- A_a activity of the artery wall

- A_b activity of lumen/blood

In cases, where the artery wall is comprised of multiple tracer-avid tissues of interest, e.g. in atherosclerotic arteries where the wall contains intimal plaque tissues in addition to regular tunica media, the wall component, A_a, can be split up into its sub-compartments. Lost activity, A_l, can also be expressed for each structure separately:

Eqn. S8:

$$A_{ROI} = \sum_{i=1}^{n} (A_{ai}) - \sum_{i=1}^{n} (A_{lai}) + A_b - A_{lb} + A_g$$

- $A_{a1..an}$ activity of arterial tissue types 1..n

- $A_{la1..lan}$ activity lost outside the ROI from tissue types 1..n due to displacement

- A_{lb} lost activity from blood due to signal displacement

The magnitude of signal that is lost outside the ROI due to signal displacement from any given arterial wall component can be expressed as a fraction of the total activity of that component:

Eqn. S9:

$$A_{ROI} = \sum_{i=1}^{n} (A_{ai}) - \sum_{i=1}^{n} (F_{lai} \cdot A_{ai}) + A_b - A_{lb} + A_g \Longleftrightarrow A_{ROI} = \sum_{i=1}^{n} [(1 - F_{lai}) \cdot A_{ai}] + A_b - A_{lb} + A_g$$

- $F_{la1..lan}$ fraction of activity of tissue types 1..n that is lost from ROI due to displacement

The above equation can be alternatively expressed in terms of the *retained* activity fraction, F_r:

Eqn. S10:

$$A_{ROI} = \sum_{i=1}^{n} (F_{rai} \cdot A_{ai}) + A_b - A_{lb} + A_g$$

- $F_{ra1..ran}$ fraction of activity of tissue types 1..n that is retained within the ROI

The magnitude of the retained signal fraction for a given arterial component depends on the distance of that component to the ROI border - the larger the distance, the larger the retained signal fraction. In arteries with small/negligible total wall thickness compared with the FWHM of the PSF, the different tissue components will display approximately equal fractional signal loss, and equivalently, the retained signal fraction would be approximately equal for all arterial tissues. In such case, the arterial signal model can be expressed as:

Eqn. S11:

$$A_{ROI} = \sum_{i=1}^{n} (F_{ra} \cdot A_{ai}) + A_b - A_{lb} + A_g$$

- F_{ra} fraction of activity of all arterial tissues

The activities can be expressed in terms of volume and activity concentrations:

Eqn. S12:

$$A_{ROI} = \sum_{i=1}^{n} (F_{ra} \cdot C_{ai} \cdot V_{ai}) + C_b \cdot V_b - \overline{C}_{lb} \cdot V_b + \overline{C}_g \cdot V_{ROI} \Longleftrightarrow A_{ROI} = \sum_{i=1}^{n} (F_{ra} \cdot C_{ai} \cdot V_{ai}) + (C_b - \overline{C}_{lb}) \cdot V_b + \overline{C}_g \cdot V_{ROI}$$

- $C_{a1..an}$ activity concentrations of tissue types 1..n

- $V_{a1..an}$ volumes of tissue types 1..n

- C_b activity concentration of blood

- V_b volume of blood

- $\overline{C}_{lb}$ lost activity concentration from blood, due to displacement (averaged for entire lumen volume)

- $\overline{C}_{g}$ gained activity concentration in ROI, due to displacement (averaged for entire ROI volume)

The volume of the lumen/blood can be expressed in terms of the difference between the ROI volume and the artery wall volume:

Eqn. S13:

$$A_{ROI} = \sum_{i=1}^{n} (F_{ra} \cdot C_{ai} \cdot V_{ai}) + (C_b - \overline{C}_{lb}) \cdot \left[V_{ROI} - \sum_{i=1}^{n} (V_{ai})\right] + \overline{C}_g \cdot V_{ROI} \Longleftrightarrow$$

$$A_{ROI} = \sum_{i=1}^{n} (F_{ra} \cdot C_{ai} \cdot V_{ai}) - (C_b - \overline{C}_{lb}) \cdot \sum_{i=1}^{n} (V_{ai}) + (C_b - \overline{C}_{lb} + \overline{C}_g) \cdot V_{ROI}$$

The blood activity that is lost outside the ROI due to signal displacement can be expressed as a fraction of total blood activity:

Eqn. S14:

$$A_{ROI} = \sum_{i=1}^{n} (F_{ra} \cdot C_{ai} \cdot V_{ai}) - (C_b - F_{lb} \cdot C_b) \cdot \sum_{i=1}^{n} (V_{ai}) + (C_b - \overline{C}_{lb} + \overline{C}_g) \cdot V_{ROI} \Longleftrightarrow$$

$$A_{ROI} = \sum_{i=1}^{n} (F_{ra} \cdot C_{ai} \cdot V_{ai}) - (1 - F_{lb}) \cdot C_b \cdot \sum_{i=1}^{n} (V_{ai}) + (C_b - \overline{C}_{lb} + \overline{C}_g) \cdot V_{ROI}$$

- F_{lb} fraction of blood activity that is lost outside the ROI due to signal displacement

The retained fraction of blood activity can be introduced:

Eqn. S15:

$$A_{ROI} = \sum_{i=1}^{n} (F_{ra} \cdot C_{ai} \cdot V_{ai}) - F_{rb} \cdot C_b \cdot \sum_{i=1}^{n} (V_{ai}) + (C_b - \overline{C}_{lb} + \overline{C}_g) \cdot V_{ROI} \Longleftrightarrow$$

$$A_{ROI} = \sum_{i=1}^{n} [(F_{ra} \cdot C_{ai} - F_{rb} \cdot C_b) \cdot V_{ai}] + (C_b - \overline{C}_{lb} + \overline{C}_g) \cdot V_{ROI}$$

- F_{rb} fraction of blood activity that is retained within the ROI

Blood activity concentration is equal for arteries and veins. Moreover, the reference vein is usually in close proximity to the artery under investigation and is therefore subject to similar signal gain from surroundings. In addition, the reference vein is usually of comparable size and anatomy. Therefore, the average signal displacement for the vein is a good estimate for that of the artery. We can, thus, combine Eqns. S15 and S6:

Eqn. S16:

$$A_{ROI} = \sum_{i=1}^{n} [(F_{ra} \cdot C_{ai} - F_{rb} \cdot C_b) \cdot V_{ai}] + \overline{C}_v \cdot V_{ROI}$$

The terms ($F_{ra} \cdot C_{ai} - F_{rb} \cdot C_b$) may be regarded as an apparent or *observed* activity concentration (C^o_{ai}):

Eqn. S17:

$$A_{ROI} = \sum_{i=1}^{n} (C^o_{ai} \cdot V_{ai}) + \overline{C}_v \cdot V_{ROI}$$

For late imaging (2-3 hours after injection) that is normally used in vascular PET [8], the tracer is almost completely cleared from blood at imaging time [9] and C_b is, thus, expected to be small/negligible compared with C_{ai}. When blood tracer concentration can be considered negligible, C^o_{ai} will be approximately equal to $F_{ra} \cdot C_{ai}$.

Calculation of tissue activity fractions

The activity fraction of a tissue component is the relative contribution of each tissue component to the total activity of the entire arterial wall:

Eqn. S18:

$$AF_{ax} = \frac{C_{ax} \cdot V_{ax}}{\sum_{i=1}^{n} (C_{ai} \cdot V_{ai})}$$

- AF_{ax} relative contribution (i.e. activity fraction) of tissue component "x" to total arterial activity
- C_{ax} activity concentration of tissue component "x"
- V_{ax} volume of tissue component "x"

Estimation of tissue activity fractions using regression analysis

When the volumes of the different arterial components are known, multi-variable regression analysis based on Eqn. S17 can be used to estimate C_{ai}^{o} for all components. Having estimated the observed activity concentrations, *estimated* activity fractions can be calculated:

Eqn. S19:

$$AF_{ax} = \frac{C_{ax}^{o} \cdot V_{ax}}{\sum_{i=1}^{n} (C_{ai}^{o} \cdot V_{ai})}$$

- C_{ax}^{o} observed activity concentration of tissue component "x"

Note that when C_b is negligible/null and when F_{ra} is approximately equal for all arterial tissue types, as outlined above, the true activity fraction (Eqn. S18) and the estimated activity fraction (Eqn. S19) will be approximately equal.

References

[1] Eschmann SM, Friedel G, Paulsen F, Reimold M, Hehr T, Budach W, Scheiderbauer J, Machulla HJ, Dittmann H, Vonthein R, Bares R. Is standardised 18F-FDG uptake value an outcome predictor in patients with stage III non-small cell lung cancer? Eur J Nucl Med Mol Imaging 2005; 33: 263-9.

[2] Lee HS, Kim HO, Hong YS, Kim TW, Kim JC, Yu CS, Kim JS. Prognostic value of metabolic parameters in patients with synchronous colorectal cancer liver metastasis following curative-intent colorectal and hepatic surgery. J Nucl Med 2014; 55: 582-9.

[3] Win T, Thomas BA, Lambrou T, Hutton BF, Screaton NJ, Porter JC, Maher TM, Endozo R, Shortman RI, Afaq A, Lukey P, Ell PJ, Groves AM. Areas of normal pulmonary parenchyma on HRCT exhibit increased FDG PET signal in IPF patients. Eur J Nucl Med Mol Imaging 2013; 41: 337-42.

[4] Nishino M, Guo M, Jackman DM, DiPiro PJ, Yap JT, Ho TK, Hatabu H, Jänne PA, Van den Abbeele AD, Johnson BE. CT Tumor Volume Measurement in Advanced Non-small-cell Lung Cancer. Acad Radiol 2011; 18: 54-62.

[5] van Kessel CS, van Leeuwen MS, Witteveen PO, Kwee TC, Verkooijen HM, van Hillegersberg R. Semi-automatic software increases CT measurement accuracy but not response classification of colorectal liver metastases after chemotherapy. Eur J Radiol 2012; 81: 2543-9.

[6] Al-Mashhadi RH, Bjørklund MM, Mortensen MB, Christoffersen C, Larsen T, Falk E, Bentzon JF. Diabetes with poor glycaemic control does not promote atherosclerosis in genetically modified hypercholesterolaemic minipigs. Diabetologia 2015; 58: 1926-36.

[7] Al-Mashhadi RH, Sørensen CB, Kragh PM, Christoffersen C, Mortensen MB, Tolbod LP, Thim T, Du Y, Li J, Liu Y, Moldt B, Schmidt M, Vajta G, Larsen T, Purup S, Bolund L, Nielsen LB, Callesen H, Falk E, Mikkelsen JG, Bentzon JF. Familial hypercholesterolemia and atherosclerosis in cloned minipigs created by DNA transposition of a human PCSK9 gain-of-function mutant. Sci Transl Med 2013; 5: 166ra1-166ra1.

[8] Bucerius J, Mani V, Moncrieff C, Machac J, Fuster V, Farkouh ME, Tawakol A, Rudd JH, Fayad ZA. Optimizing 18F-FDG PET/CT imaging of vessel wall inflammation: the impact of 18F-FDG circulation time, injected dose, uptake parameters, and fasting blood glucose levels. Eur J Nucl Med Mol Imaging 2013; 41: 369-83.

[9] Iozzo P, Gastaldelli A, Järvisalo MJ, Kiss J, Borra R, Buzzigoli E, Viljanen A, Naum G, Viljanen T, Oikonen V, Knuuti J, Savunen T, Salvadori PA, Ferrannini E, Nuutila P. 18F-FDG assessment of glucose disposal and production rates during fasting and insulin stimulation: a validation study. J Nucl Med 2006; 47: 1016-22.